

Phase Transition of the single-layer vanadium diselenide on Au(111) with distinguished electronic structures

Jinbang Hu, Xiansi Wang, Chaoqin Huang, Fei Song, and Justin W Wells

Jinbang Hu

Department of Physics, Norwegian University of Science and Technology, NO-7491

Trondheim, Norway

E-mail: jinbang.hu@ntnu.no

Xiansi Wang

Hunan University, Changsha, 410082, China

Fei Song, Chaoqin Huang

Shanghai Advanced Research Institute, Chinese Academy of Sciences, Shanghai 201000,

China;

Justin W. Wells

Department of Physics, Norwegian University of Science and Technology, NO-7491

Trondheim, Norway

Semiconductor Physics, Department of Physics, University of Oslo (UiO), NO-0371 Oslo,

Norway

Keywords: phase transition, 2D material

Abstract

Herein, we report the reversible structure transition of the single-layer VSe_2 grown on Au (111) with the alternating thermal annealing and Se replenishment. Using scanning tunnelling microscopy (STM) and angle-resolved photoemission spectroscopy (ARPES), we demonstrate the epitaxially growth of high-quality VSe_2 on Au (1 1 1) with the octahedral (1T) structure and the Se-vacancy-induced structure transformation of VSe_2 from the metallic Morrie (1T) phase to the semiconducting (2H) phase with an increased in-plane lattice constant. With the convincing agreement between the experimental results and DFT calculations, the nanostructure near the gain boundary in the defective intermediate phase is confirmed, as well as the reaction pathway with Se gradually depleted at elevated temperatures. It is revealed that the Se density of the line-shape defects plays an important role in the formation of the 2H domain phase, due to the increment of the in-plane lattice parameter after the Se desorption, and the better thermal stability of 2H phase compared to the 1T phase. Importantly, the proper control of the density of Se could feasibly manipulate the

ratio between the 1T and 2H phase in the steak domain, which is regarded as a good platform for the 2D homojunctions in nanoelectronics.

1. Introduction

Artificial two-dimensional (2D) van der Waals structures, shows great promise in designing novel electronic and optoelectronic devices^[1]. So far, considerable efforts have been devoted not only to investigating fundamental properties but also to exploring the engineering strategies to modify local phase transitions in 2D materials, with the goal of realizing controllable design of homojunctions^[2]. Atomically thin 2D materials such as transition metal dichalcogenides (TMDs)^[3], graphene^[4] and graphene analogues^[5] have also been credited with unique properties, including valley-polarized exciton^[6], 2D ferromagnetism^[7], and room-temperature ferroelectricity^[8]. In the post-Moore era, a variety of strategies such as vapor-phase deposition^[9], laser irradiation^[2a, 10], chemical doping^[11], and doping engineering^[12], have been adopted for realizing controllable construction of 2D homojunctions.

Apart from the heterojunctions constructed by two different materials, TMDs with the natural matching of chemical and electronic structures in different polymorphic phases (e.g. 1T, 2H) provide a convenient platform for fabricating 2D homojunctions, which usually have a continuous band bending and a high-quality carrier transport and separation at the interface^[2b]. Specifically, phase-engineered metallic 1T-MoS₂/semiconducting 2H-MoS₂^[13] and metallic 1T'-MoTe₂/semiconducting 2H-MoTe₂^[2a] were reported with low-resistance contacts and improved carrier mobility. Hence, the actual dynamical process of the transformation between 1T and 2H phases and its boundary structures must be corroborated in constructing 2D heterostructures homojunctions.

Here, we report the synthesis of epitaxial SL VSe₂ on Au (1 1 1) and provide in-situ observations of the phase transformation process from pristine homogeneous 1T phase passing through a defective 2H domain phase, end in a VSe stripe phase decorated by Se line upon annealing at elevated temperature. Our study applies a diverse set of characterization Methods, combining STM with ARPES to exhibit the difference between 1T and 2H phases. Throughout the exposition we use density functional theory (DFT) calculations to account for the observations. We discussed the structure reaction pathway determined by the loss of Se induced in-plane increased lattice structure, which will facilitate future precisely artificial two-dimensional (2D) van der Waals structures as desired homojunctions.

2. Experiment details and calculation methods

All sample preparation steps and experiments were performed under ultrahigh vacuum conditions better than 4×10^{-10} mbar. The Au (111) surface was prepared by repeated sputtering and annealing cycles. The quality of the clean surface was confirmed by the well-known Au-herringbone reconstruction in STM observation and the intensity of the surface state, i.e., the Shockley state (see Figure. s1 in the Supplemental Material). Subsequently, Se (purity 99.9999%) and V (purity 99.99%) were co-deposited onto the clean surface at 300 °C, yielding a pure 2D Morrie structure at around 1 ML. Then the prepared monolayer VSe₂ was further annealing at elevated temperature up to 460 °C, the different structure formation after the sample preparation was confirmed by LEED and STM observation, and also the corresponding band structure measurements. The lab based ARPES

measurements were performed at RT using an aberration-corrected, energy-filtered photoemission electron microscope (EF-PEEM) (NanoESCA III, Scienta Omicron GmbH) equipped with a focused helium discharge lamp primarily generating He I photons at $h\nu = 21.22$ eV. Pass energy $EP=25$ eV and a 0.5 mm entrance slit to the energy filter was used^[14], yielding nominal energy and momentum resolutions of $\Delta E = 50$ meV and $\Delta k=0.02 \text{ \AA}^{-1}$.

The density functional theory (DFT) calculations were performed using the Vienna Ab initio Simulation Package (VASP)^[15]. The interactions between the valence electrons and ion cores were described by the projector augmented wave method^[16]. The electron exchange and correlation energy was treated by the generalized gradient approximation with the Perdew-Burke-Ernzerhof functional^[15, 16b]. The kinetic energy cutoff of the plane-wave basis was set to 500 eV as default. A $5 \times 5 \times 1$ supercell of 1T phase on a Au (111) substrate was considered to study the effect of moiré superstructure. The STM simulations are performed using the Tersoff–Hamann approach^[17]. The band dispersion for the freestanding single layer 1T, 2H and VSe buckling phase were calculated without spin-orbital coupling (SOC), respectively. All the structures were optimized until the forces on the atoms were less than 20 meV \AA^{-1} . The vacuum layer is thicker than 15 \AA applied to eliminate spurious interaction between two adjacent slabs.

3. Discussion

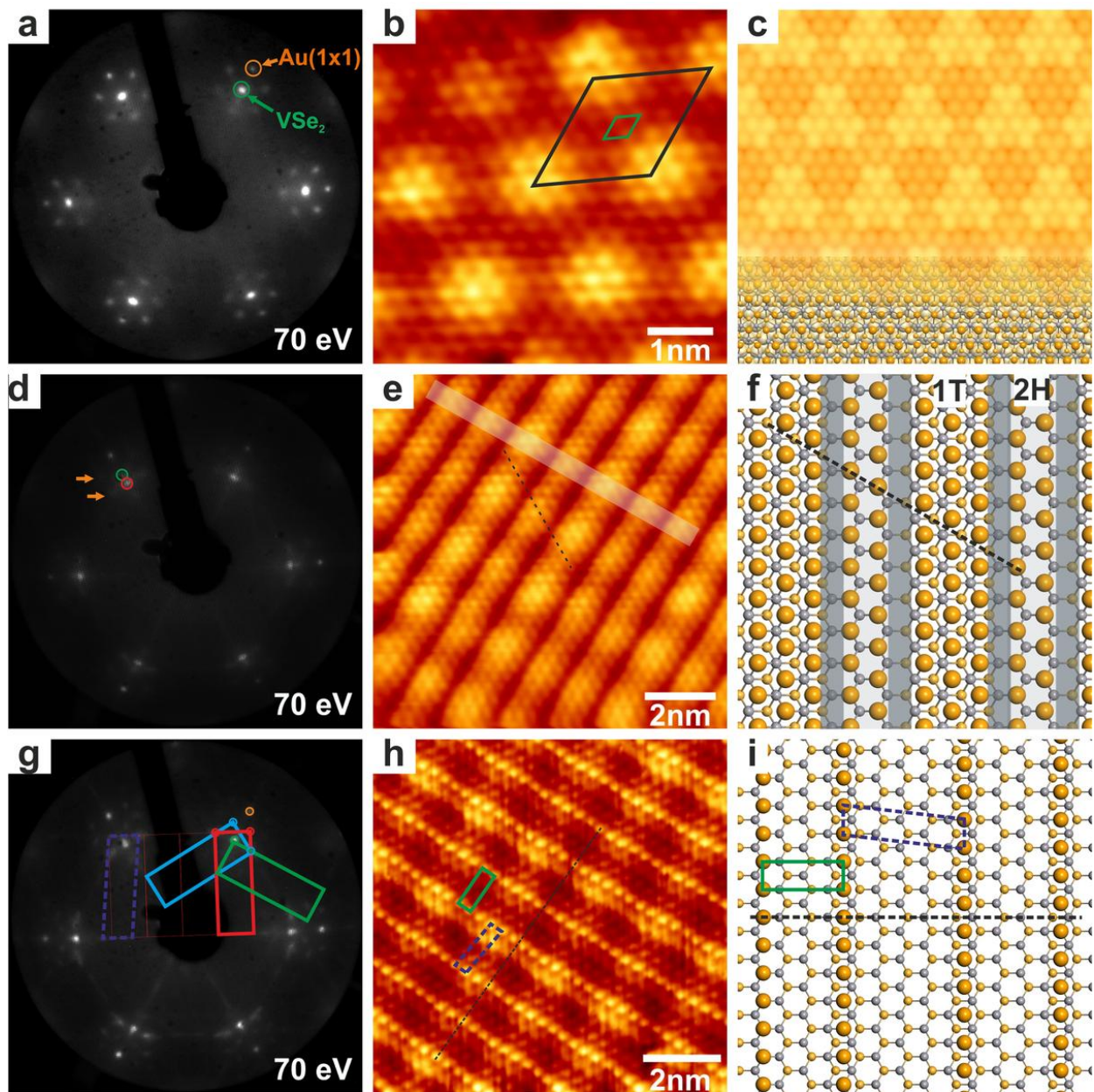


Figure 1. Evolution of the crystal morphology of single-layer VSe_2 on $\text{Au}(1\ 1\ 1)$ at elevated temperature. Top row shows (a) LEED pattern (70 eV), (b) STM observations and corresponding energetically favourable atomic model(c) of epitaxially grown VSe_2 monolayer at 300 $^\circ\text{C}$, the STM simulation overlaid on the top side of image (c). The middle row and the bottom row show further annealing to 380 $^\circ\text{C}$ (d-f) and 460 $^\circ\text{C}$ (g-h), respectively. The circles in (b) show the positions of LEED spots for VSe_2 monolayer before (green circle) and after annealing to 380 $^\circ\text{C}$ (yellow circle). The corresponding unit cells of the selenide line-shaped reconstruction in (g-h) are indicated by the rectangular and dashed parallelogram. The black dashed line in (e,f,h,i) are used to compare the relative position of topmost Se. Scanning parameters: (b) 1 V, 1.0 nA; (e) -1.2V,6.9 nA; (h) -1.2V,8.4 nA;

Figure 1 depicts a general overview of three different phases obtained in epitaxially grown VSe_2 monolayer at 300 $^\circ\text{C}$, and subsequently annealing to 380 $^\circ\text{C}$ and 460 $^\circ\text{C}$ as demonstrated, respectively, by LEED patterns and STM images. Initially, VSe_2 monolayer was fabricated by Se and V co-deposited onto the clean surface at 300 $^\circ\text{C}$. From the LEED panel of Figure 1a, a clear moiré pattern surrounding the main spots of the VSe_2 atomic lattice coincide with the $\text{Au}(1\times 1)$ diffraction spot indicates a possible commensuration between a (6×6) reconstruction of the Au (111) substrate with the apparent moiré corrugation with a (5×5) superlattice of the as-grown VSe_2 , which is in agreement with the STM observation shown in Figure 1b. On the basis of this STM data, the atomic lattice constant of the moiré superstructure has a lattice parameter of 17.7 \AA , while the atomic lattice parameter is 3.45 \AA ,

as the unit cell marked by the black and green rhombus in Figure 1b, respectively. To further investigate the atomic structure of VSe_2 on Au (111), we employed DFT calculations to construct an optimized 5×5 structural model of the 1T- VSe_2 on Au substrate, as depicted in Figure 1c. The corresponding STM simulated image show a periodic moiré structure, in agreement with STM data. The model of 1T- VSe_2 applied here based on our ARPES measurement, which will be discussed below.

Annealing the samples to 380°C described in middle row of Figure 1 induces the phase transition as evidenced from the LEED pattern (Figure 1d), in which shows an additional hexagonal lattice (marked by red circle) with a slightly smaller reciprocal lattice constant than that of as grown 1T phase (marked by green circle), and the corresponding moiré spots (marked by yellow arrow) was mostly disappeared. Meanwhile, the STM image of Figure 1e reveals a different appearance in the moiré patterns and clearly visible lines of the defect decorated in the SL VSe_2 . The density of the line-shaped defects relates to the annealing temperature, as discussed in Ref^[18] We emphasize that this new appearing moiré structure (marked by the white ribbon in Figure 1e) in the defective structure of SL VSe_2 originates from the Au-herringbone reconstruction, which can be clearly clarified in Figure 2a of ref^[18], since the moiré structure in dislocation-dominated defective VSe_2 appears without commensurating relation to the line-shaped defects. We then deduce the new appearing moiré structure is caused by the interaction between Au surface and defective VSe_2 monolayer. Moreover, the topmost Se atom seems to be rearranged in two adjacent steak-shaped domains, as indicated by the black dashed line in Figure 1e. The dashed line goes through the top site of Se in one steak-shaped domain while through the bridge site of Se atom. We proposed a possible structure model (Figure 1f) with 1T and 2H phase coexist in the defective VSe_2 monolayer, as the line of Se defect marked by the grey ribbon to separate two different phase, much like what has been seen previously in Se vacancies rearrangement mediate the transformation from 1T domains to 2H domains^[9b, 19]. The further confirmation of the existence of 2H phase will be given in the discussion of ARPES data and STM observation as below.

The completed transition to a striped phase is seen after annealing to 460°C and is shown in bottom row of Figure 1. The atomically resolved STM image, shown in Figure 1h, reveals the line-shaped rearrangement of the Se atom with a rectangular unit cell for two nearest bright line of atoms, while a parallelogram unit cell for two bright line with the shift of half a unit cell along the direction of the line of Se atoms. The experimentally observed shift can be clearly identified by the black dashed guideline in STM image 1h. Correspondingly, The LEED data of striped phase in Figure 1g exhibits a complicated diffraction pattern which is much like what has been observed previously in similarly prepared SL VSe_2 on Au(111)^[20]. Taking into account the unit cell of the structure identified by STM, the diffraction spots (marked by colourful circles) in LEED pattern can be reproduced by the reciprocal rectangular unit cells deriving from the three rotational domains. Moreover, the expected LEED spots from the reconstruction of Se atoms as bright line appears to be broadening along the short side of the rectangular unit cells, which can be explained by the parallelogram unit cell for two bright Se line with the shift of half a unit cell, marked as dashed parallelogram in both Figure 1g and 1h, respectively. Based on the analysis of the LEED data and STM observation, an optimized structural model of VSe_2 with the line of Se decorated on the top as a defective phase of VSe_2 was constructed. Obviously, the topmost Se atom in the line-shaped array could stack on the top site or hcp site with regard to the bottom layer of Se atom. The

parallelogram unit cell for two bright Se line with the shift of half a unit cell revealed in the STM observation indicates the corresponding two adjacent line of Se atom have the same stacking style, while the rectangular unit cell and the ratio between the two side of rectangular indicates one of the line-shaped Se array stack like 1T phase and another line of Se atom stack like 2H phase. Hence, the two different stack style of the Se lines revealed here also indicates the possible transition of 1T phase to 2H phase in local steak-shaped domain separated by the line of the Se defects. Moreover, comparing to the LEED pattern of the as-grown SL VSe₂ with a periodic moiré structure, the slightly shrunk reciprocal rectangular unit cell indicates that VSe with Se line stacked on the top has an expanded in-plane lattice constant after an obvious Se depletion caused by heating the VSe₂ layer in vacuum.

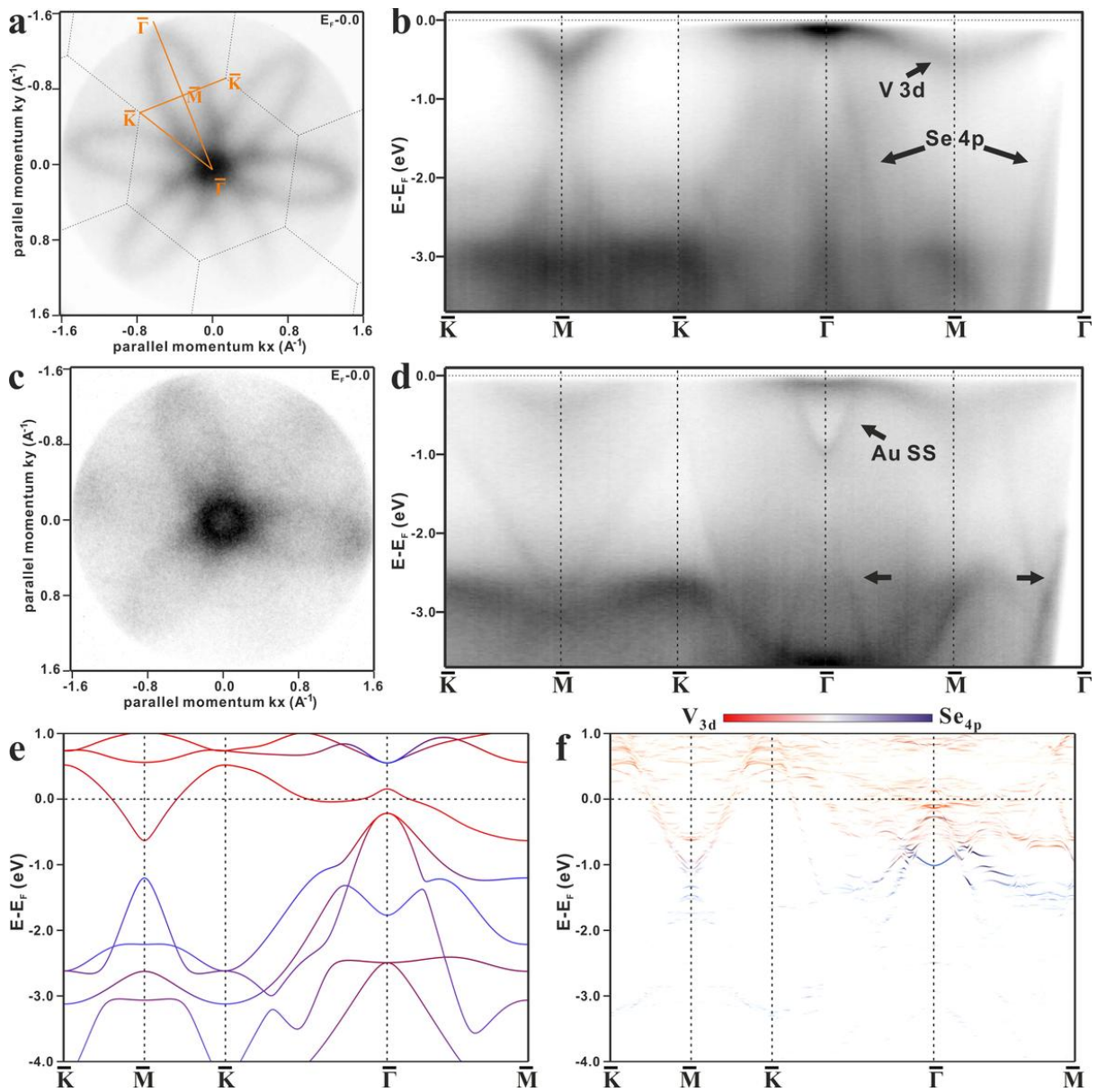


Figure 2. Electronic structure of as-grown SL VSe₂ on Au(1 1 1) and upon heating to 380 C°. Fermi surface (a) and band dispersion (b) along the high symmetry lines of the as-grown SL VSe₂ with the moiré superstructure measured ($h\nu = 21.2$ eV) at room temperature. (c) and (d) Same as (a) and (b), but for the steaked-VSe₂ (heating to 380 C°) decorated by line of Se defect. The dashed hexagon in (a) represents the 2D Brillouin zone (BZ) with symmetry point labels overlaid. A few observations of particular interest are indicated by arrows. A nonmagnetic calculated band structure of the SL 1T-VSe₂ without (e) and with (f) Au substrate induced moiré superstructure being considered for the model. The different atomic orbital contributions are color coded.

ARPES measurements has been applied to track the electronic structure of the several phases observed in STM image upon heating. Figures 2a and 2b show the fermi surface and band dispersion along the high symmetry lines of the as-grown SL VSe₂, respectively. The new features (pointed by black arrow) appear to be periodic with respect to the unit cell of SL VSe₂. The overall band dispersions observed experimentally are entirely consistent with the reported band feature of SL 1T-VSe₂ grown on a HOPG substrate^[21] and the nonmagnetic calculation of the SL 1T-VSe₂, as shown in Figure 2e. Based on the orbital-projected band structures of the V3d and Se 4p orbitals, the Fermi surface which forms closed flower-like contours was confirmed to be dominated by the V 3d-derived band crossing Fermi level(E_f) as electron-like conducting band, and the parabolically dispersing band mainly from Se 4p orbital extends steeply down from the Γ point into the lower lying valence band. We deduce the relatively fuzzy feature of the band dispersion originates from the periodic moiré structure of SL VSe₂, the DFT calculation neglecting the spin-orbit coupling (SOC) effects was performed using a 5x5 supercell of SL VSe₂ on Au substrate with a periodic moiré structure, concluded from LEED and STM data. Figure 2f shows the calculated band structure with the contributions from V 3d and Se 4p states. The projected band feature near the E_f shows a similar dispersion like the system of free standing SL VSe₂, but exhibit a broadening character, which indicates the moiré structure induces distortion in the SL VSe₂ partly contributes to the fuzzy feature.

Upon heating to 380 C°, Figures 2c and 2d show the fermi surface and band dispersion of the steaked phase decorated by line of Se defect (shown in Figure 1e). Comparing with the ARPES data recorded of as-grown homogeneous 1T phase, the band structure originating from the SL 1T-VSe₂ becomes weaker and several new band features appear, marked by the black arrow in Figure 2d. The weak band feature near the E_f like the as-grown 1T phase indicates there are still domain of 1T phase remaining in the defective SL VSe₂ network. However the new parabolically band appears with the whole feature at 2eV below the E_f , which is extremely different from the parabolically Se 4p -derived band in 1T phase dispersing with the band top near the E_f . Meanwhile, our DFT calculated band structure of 1T phase with increased in-plane lattice constant observed in defective steak phase indicates the energy position of the parabolically dispersing band (marked by black arrow) mainly from Se 4p orbital seems to be rarely influenced as a comparison with the band structure of the homogeneous 1T phase (Figure s2). Based on the new parabolically band appearing deeply 2eV below the E_f while the V 3d-derived band of defective 1T-VSe₂ domain remains crossing E_f with rarely energy shift caused by charge transfer from the Au substrate, we then deduce this new parabolically band feature originates from a new phase upon annealing. In addition, there is a parabolically electronic pocket appearing around the Γ point with the bottom at -1.0 eV, which is a typically band feature of the Shockley state from the clean Au (111). The Shockley state observed in ARPES measurement indicates the moiré structure of dislocation-dominated defective VSe₂ recorded in STM observation originates from the interaction with the typical herringbone reconstruction of Au (111) surface.

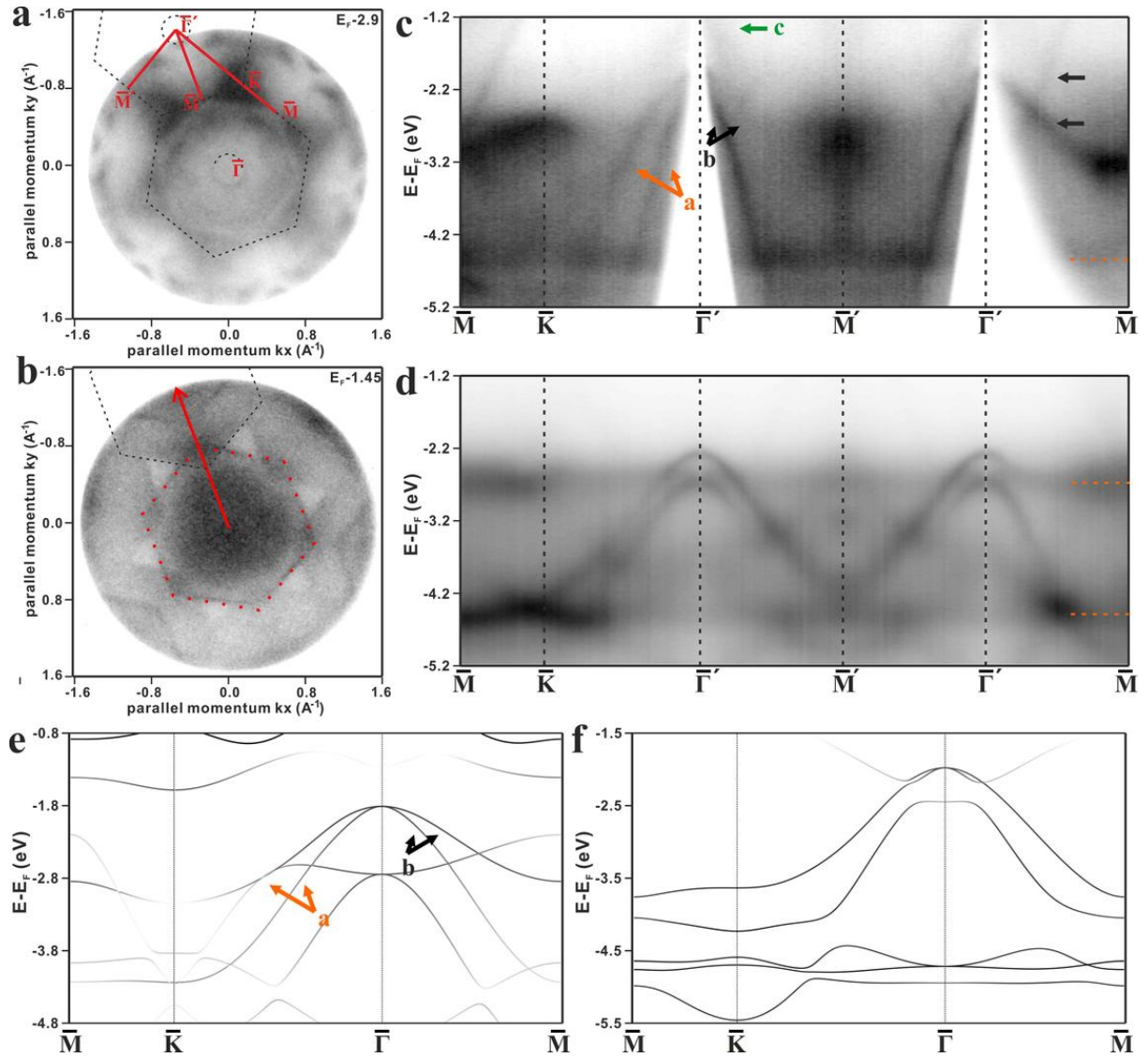


Figure 3. Electronic structure of defective SL VSe₂ upon heating to 450 °C (a-c) and 460 °C (d). Constant-energy contours at -2.9eV with 2D BZ of defective SL VSe₂ shown in black dashed hexagon, (b) Constant-energy contours at -1.45eV shows the Umklapp scattering process of Au sp band. The original(scattering) Au sp band marked by the red(black) dashed hexagon. The reciprocal lattice vectors marked as red arrow indicate one of the possible Umklapp scattering direction. (c) band structure recorded on the high symmetry directions marked by the red line in (a). (d) Same as (c), but for striped-VSe (heating to 460 °C) decorated by line of Se on the top. The position of flat bands in (c) and (d) are indicated by yellow dashed line. the V 3d projected band structure of the SL 2H-VSe₂ (e) and SL VSe (f) without SOC being considered for the calculation.

To further explore the origin of the new band feature in the steaked VSe₂, a comparative study between the electronic structure of steaked VSe₂ from ARPES measurement and the calculated band structure of the SL 2H-VSe₂ can be used to identify the new phase formed in the different domains separated by line of Se defect. Figure 3a-b shows the constant-energy contours at -2.9eV and -1.45eV below the E_f , the band feature shows sixfold symmetry, which indicates the different domains in the steaked VSe₂ has a similar hexagonal lattice structure. Specifically in Figure 3b, a careful analysis of the hexagon shaped band feature, marked by the dashed line, reveals the Umklapp scattering process of Au sp band with the reciprocal lattice vectors (red arrow) of the steaked phase. Based on only one type of reciprocal lattice vector with six fold symmetry, the proposed 2D surface BZ of defective SL VSe₂ was overlaid on the constant-energy contours at -2.9eV by black dashed hexagon (Figure 3a). Moreover, comparing to the sp band feature from Au substrate(Figure s1), we deduced the lattice parameter of the domain in steaked phase is hexagonal unit cell with lattice vector 3.65 Å, which is in agreement with an increased lattice parameter observed from LEED and STM

data. However, a first-principles calculations from the SL 1T-VSe₂ with increased lattice vector 3.65 Å (Figure s2c) has consistently predicted the band features near the E_f, not the new parabolically band feature appearing deeply 2eV below E_f. Hence a possible candidate, 2H-VSe₂, has been considered, since constant-energy contours in Figure 3a and 3b confirmed only one hexagonal unit cell in steaked phase. Additionally, the similar phase transition has been reported in MoS₂, MoSe₂, MoTe₂ and PtSe₂^[2a, 9b, 19, 22]. Figure 3c shows the band dispersion along the high symmetry directions, marked by the red line in Figure 3(a). The parabolically bands with two branches along the Γ -M and Γ -K direction, labelled as 'a' and 'b', disperse separately away from the Γ point. The calculated bands of the SL 2H-VSe₂ without SOC, as displayed in Figure 3e, exhibit a overall good agreement with the experimental bands 'a' and 'b' in Figure 3c. As we discussed above, the typically V 3d-derived band losing partially of their spectral weight remains crossing E_f confirms the existence of 1T phase in the steaked domain, and the new clear band feature deeply 2eV below E_f can be explained by our DFT predicted band structure of 2H phase with increased lattice instead of 1T phase, we then deduce the phase transition from as grown homogeneous 1T phase to coexistence of 1T and 2H domains randomly distributing in the defective steaked phase. Note that, the clear V3d derived band feature of 1T phase near the E_f shows rarely energy shift referring to the calculated SL 1T phase without substrate, while the V3d derived band of 2H phase is located at a slightly higher binding energy of 0.8eV. This may reflect a electron doping of 2H domains due to charge transfer from the substrate, since 1T phase of VSe₂ has been reported to be metallic and 2H phase shows like a semiconductor^[23].

Annealing in UHV at higher temperatures 460C° leads to a transition from the steaked phase to a striped phase in our STM observation. we speculate that it might be a buckling VSe network decorated by lines of Se atom which results from losing almost all of the Se atom at the top layer of VSe₂ at higher temperature. Correspondingly in Figure 3d, the band dispersion along the high symmetry directions has been experimentally recorded to study additional information of the proposed VSe network. Obviously, two similar parabolical band disperse to a maximum energy at the Γ point with a direct gap 0.45eV, which is obviously different from the band dispersion of the steaked phase in Figure 3c. A nonmagnetic calculation of the simplified VSe network (Figure 3f) without the doping by line of Se atoms reveals a band dispersion quite similar to our ARPES measurements, except that there one non-dispersive bands (marked by yellow dotted lines) at -2.6 eV coinciding with the maximum of the lower parabolic band and another one at -4.5 eV. Since these nondispersive bands remaining after a phase transition from from the steaked phase to a striped phase, we assume these flat bands may origin from surface resonant states that mix with bulk bands (or bulk bands projection)^[24]. The overall agreement between experimental and calculated band dispersions as well as our analysis of the model based on STM observation indicates a buckling VSe network formed with the significant depletion of almost all Se at top layer of VSe₂ upon heating. Comparing to the initial prepared 1T-VSe₂ with the moiré superstructure, we experimentally find an increasing tendency of the lattice parameter during the structure transformation in our ARPES measurement-consistent with the observations from LEED and STM. Note that, the overall band structure of VSe striped structure rigidly shift in our ARPES measurement as a comparison to the calculation of SL VSe without the Au substrate and doping of Se arrays considered, similar to what has been observed in hBN on Ir(111)^[25].

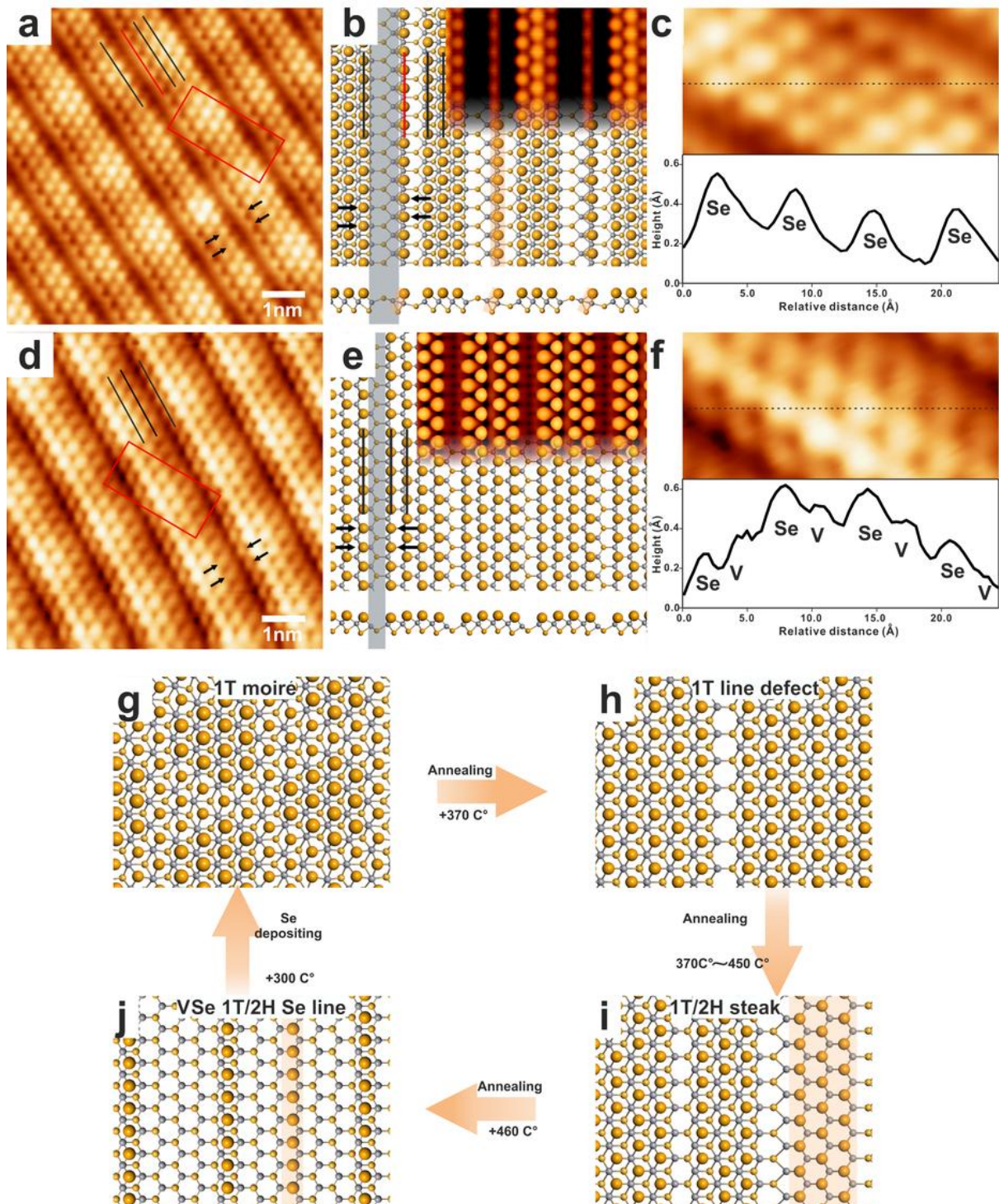


Figure 4. Atomically resolved STM of two different striped pattern(a,d) upon heating and Schematic illustration of the structural transformation from pure 1T VSe_2 to 1T/2H patterned VSe_2 (g-i). (a) STM observation of the 1T steaked phase decorated by the line of Se defect, (b) the proposed energetically favourable atomic model with simulated STM image overlaid to the top right side of the model. (c-d) same as (a-b) but for the 2H steaked phase. The relative Se atom position in different steak domain near the sides of line-shaped defect is marked by black arrow in (a,b,d,e), respectively. Four short line near the top of STM image (a,d) used to mark the width of the line-shaped defect, corresponding to the gray shadow in (b,e). (c) and (f) Enlarged image of the region indicated by the red rectangle in image (a) and (d). The intensity profile along the black dashed line is overlaid on the image. Scanning parameters: (a) -1.2 V, 6.9 nA; (d) -1.2V, 1.0 nA.

On the basis of the above experimental data, STM and ARPES measurements reveal three distinct crystalline phases. Specifically, the as-grown 1T- VSe_2 with periodic moiré structure and the complete transition to buckling VSe stripe phase has been clearly discussed. However, the intermediate phase, dislocation-dominated defective VSe_2 , has been confirmed to be a coexistence of 1T and 2H domain from our analysis of ARPES result. Gaining an

understanding of the coexisted steaked domain remains unclear and is important for the scenario of artificial designing two-dimensional (2D) van der Waals structures based on transformation mechanism. Here, atomically resolved STM image reveals two different steaked structure in Figure 4a and 4d, together with the optimized configurations in Fig. 4b and 4e. We refer to the two different steaked phase as ‘phase I and II’ shown in Figure 4a and 4c, respectively. At the first glimpse, the domain of phase I exhibits bright one edge protrusions and faint another edge, which indicates the structure near the two sides of the steak domain in phase I are different. And the phase II, by contrast, displays brighter in the middle than the two side of the edges. Moreover, a careful analysis the relative Se position within the steak domain(indicated by the black arrow in STM image), we experimentally find that the Se atom at the one side of defective line shows a half unit cell shift along the direction of defective line regarding to the Se atom at another side in phase I, while no obvious relative shift of the Se atom at the two side of defective line in phase II. Combined with the line of Se defect in phase II display more narrow than phase I, as indicated by the four short line near the top of STM image, We deduce the adjacent steaked domains in phase I are separated by one line of Se defect, while the adjacent domains separated by two adjacent line of Se defect in phase II.

Interestingly, comparing the two enlarged steaked domain phase in Fig. 4(c) and (4f), the intensity profile across the domain in the upper level of the corresponding figure shows obvious difference where alternate Se-V peaks are observed on the domain of phase I and only Se peaks are observed on the phase II, much like the as grown 1T phase(Figure 3s) and what has been seen previously in similarly prepared SL MoS₂, MoSe₂ and PtSe₂[^{2a, 9b, 19, 22}]. Moreover, the consistent hexagonal and honeycomb features is also confirmed in our STM simulation of free standing SL 1T and 2H phase, respectively(Figure 3s). Combined with our ARPES confirmation of the coexistence of 1T and 2H phase, we deduced the steak domain with line of Se defect in phase I is 1T phase, and phase II is 2H phase. Based on our discussion of the relative position of Se atom near the line shaped defect, the corresponding energetically favourable atomic model are proposed in Figure 4b and 4e. Simulation of the STM image based on the proposed model, showing overall good agreement with the atomic resolution STM image (Figure 4a and 4d), especially a bamboo shaped feature of the line of Se atoms at the one side of steak domain in phase I(marked by the red line in Figure 4a) reproduced in the simulated image(top right of Figure 4b). A likely explanation for this abnormal distorted feature at the boundary of one side of steak domain is this array of Se atom at a transition state between 1T phase and 2H phase, due to a higher electronic contribution from V atom in 2H phase distributing between the two adjacent Se atoms.

Atomic mechanism of the phase transition from the homogeneous 1T phase to the striped phase of VSe network with the line of Se decorated are presented in Figure 4g-i. Specifically, thermal annealing of as-grown 1T structure VSe₂ film at an elevated temperature leads to the loss of top-layer Se atoms to form a defective structure, accompanied by an increased lattice constant. An increasing desorption of the Se atoms from the top layer has a significant impact on the rearrangement of the remaining atoms in different domain phase. The local steak domain separated by the line of Se defect would keep the 1T phase when small amount Se desorption occurs, since the lattice constant rarely changes. Furthermore, the arrangement of remaining Se atoms to form the domain in 2H phase occurs after an increasing Se desorption, which indicates the 2H phase is more stable in a slightly larger lattice unit cell than the unit cell for homogeneous 1T phase. Heating to 460 °C leads to a complete phase transformation from steak phase to a VSe network with small amount of Se decorated on the top (Figure 4i), and this structure can, of course, again be transformed into pristine defect-free 1T phase by adding Se atoms while annealing the sample to 300C° in vacuum^[18]. We then conclude that the density of the line shaped Se defects plays an important role in the formation of 2H

domain phase, due to the lattice parameter of defective structure increased after Se desorption, and the thermal stability of 2H phase is better than 1T phase with an increased lattice unit cell. Hence, proper control for the density of Se atoms by thermal annealing and readding Se atoms could adjust the ratio between 1T and 2H phase in the steak domain.

4. Conclusion

In conclusion, we have reported phase transition from the initial homogeneous 1T phase fabricated on Au (111) passing through a defective 1T/2H coexisted intermediates prior to formation of the final striped VSe network. Characterizations by STM, ARPES, and their agreement with DFT calculations elucidated the difference in the electronic structures between 1T phase and 2H phase. Our study the defective structure near the boundary between two VSe₂ domains reveals the dynamics of defect movement and rearrangement behavior of the remaining Se atom at the top site. we found that the desorption of the Se atom leads to the defective lattice formed with an increased lattice parameters, which is more stable for 2H phase at high temperatures. Moreover, the reversible phase transition pathway indicates the proper control for the density of Se atoms by thermal annealing and readding Se atoms can be regard as a good method for artificial the 2D van der Waals structures as homojunctions.

Supporting Information

Supporting Information is available from the Wiley Online Library or from the author.

Acknowledgements

This work was partly supported by the Research Council of Norway, Projects No. 324 183, No. 315 330, No. 323 766, and No. 262 633. The STM measurement was financially supported by the National Key Research and Development Program of China (2021YFA1600800) and National Natural Science Foundation of China (11874380, 22002183). The DFT calculations in collaboration with X.S. Wang supported from the National Natural Science Foundation of China (Grants No. 11804045 and 12174093) and the Fundamental Research Funds for the Central Universities.

Reference

- [1] a) Q. H. Wang, K. Kalantar-Zadeh, A. Kis, J. N. Coleman, M. S. Strano, *Nature Nanotechnology* **2012**, 7, 699; b) K. S. Novoselov, A. Mishchenko, A. Carvalho, A. H. Castro Neto, *Science* **2016**, 353, aac9439.
- [2] a) S. Cho, S. Kim, J. H. Kim, J. Zhao, J. Seok, D. H. Keum, J. Baik, D.-H. Choe, K. J. Chang, K. Suenaga, S. W. Kim, Y. H. Lee, H. Yang, *Science* **2015**, 349, 625; b) F. Wang, K. Pei, Y. Li, H. Li, T. Zhai, *Advanced Materials* **2021**, 33, 2005303.
- [3] S. Manzeli, D. Ovchinnikov, D. Pasquier, O. V. Yazyev, A. Kis, *Nature Reviews Materials* **2017**, 2, 17033.
- [4] a) K. S. Novoselov, V. I. Fal'ko, L. Colombo, P. R. Gellert, M. G. Schwab, K. Kim, *Nature* **2012**, 490, 192; b) A. K. Geim, K. S. Novoselov, *Nature Materials* **2007**, 6, 183.
- [5] F. Reis, G. Li, L. Dudy, M. Bauernfeind, S. Glass, W. Hanke, R. Thomale, J. Schäfer, R. Claessen, *Science* **2017**, 357, 287.
- [6] P. Rivera, K. L. Seyler, H. Yu, J. R. Schaibley, J. Yan, D. G. Mandrus, W. Yao, X. Xu, *Science* **2016**, 351, 688.
- [7] a) D. J. O'Hara, T. Zhu, A. H. Trout, A. S. Ahmed, Y. K. Luo, C. H. Lee, M. R. Brenner, S. Rajan, J. A. Gupta, D. W. McComb, R. K. Kawakami, *Nano Letters* **2018**, 18, 3125; b) Z. Zhang, J. Shang, C. Jiang, A. Rasmita, W. Gao, T. Yu, *Nano Letters* **2019**, 19, 3138.
- [8] a) S. Yuan, X. Luo, H. L. Chan, C. Xiao, Y. Dai, M. Xie, J. Hao, *Nature Communications* **2019**, 10, 1775; b) K. Chang, J. Liu, H. Lin, N. Wang, K. Zhao, A. Zhang, F. Jin, Y. Zhong, X. Hu, W. Duan, Q. Zhang, L. Fu, Q.-K. Xue, X. Chen, S.-H. Ji, *Science* **2016**, 353, 274.
- [9] a) J. H. Sung, H. Heo, S. Si, Y. H. Kim, H. R. Noh, K. Song, J. Kim, C.-S. Lee, S.-Y. Seo, D.-H. Kim, H. K. Kim, H. W. Yeom, T.-H. Kim, S.-Y. Choi, J. S. Kim, M.-H. Jo, *Nature Nanotechnology* **2017**, 12, 1064; b) X. Lin, J. C. Lu, Y. Shao, Y. Y. Zhang, X. Wu, J. B. Pan, L. Gao, S. Y. Zhu, K. Qian, Y. F. Zhang, D. L. Bao, L. F. Li, Y. Q. Wang, Z. L. Liu, J. T. Sun, T. Lei, C. Liu, J. O. Wang, K. Ibrahim, D. N. Leonard, W. Zhou, H. M. Guo, Y. L. Wang, S. X. Du, S. T. Pantelides, H. J. Gao, *Nature Materials* **2017**, 16, 717.
- [10] Y. Yu, M. Ran, S. Zhou, R. Wang, F. Zhou, H. Li, L. Gan, M. Zhu, T. Zhai, *Advanced Functional Materials* **2019**, 29, 1901012.
- [11] a) G. Eda, H. Yamaguchi, D. Voiry, T. Fujita, M. Chen, M. Chhowalla, *Nano Lett* **2011**, 11, 5111; b) J. Wu, J. Peng, Y. Zhou, Y. Lin, X. Wen, J. Wu, Y. Zhao, Y. Guo, C. Wu, Y. Xie, *Journal of the American Chemical Society* **2019**, 141, 592.
- [12] a) D. Xiang, T. Liu, J. Xu, J. Y. Tan, Z. Hu, B. Lei, Y. Zheng, J. Wu, A. H. C. Neto, L. Liu, W. Chen, *Nature Communications* **2018**, 9, 2966; b) N. Liu, H. Tian, G. Schwartz, J. B. H. Tok, T.-L. Ren, Z. Bao, *Nano Letters* **2014**, 14, 3702.
- [13] R. Koppera, D. Voiry, S. E. Yalcin, B. Branch, G. Gupta, A. D. Mohite, M. Chhowalla, *Nature Materials* **2014**, 13, 1128.
- [14] M. Escher, N. Weber, M. Merkel, B. Krömker, D. Funnemann, S. Schmidt, F. Reinert, F. Forster, S. Hüfner, P. Bernhard, C. Ziethen, H. J. Elmers, G. Schönhense, *Journal of Electron Spectroscopy and Related Phenomena* **2005**, 144-147, 1179.
- [15] A. Görling, *Physical Review A* **1999**, 59, 3359.
- [16] a) G. Kresse, D. Joubert, *Physical review b* **1999**, 59, 1758; b) P. E. Blöchl, *Physical Review B* **1994**, 50, 17953.
- [17] J. Tersoff, D. R. Hamann, *Physical Review B* **1985**, 31, 805.
- [18] C. Huang, L. Xie, H. Zhang, H. Wang, J. Hu, Z. Liang, Z. Jiang, F. Song, *Nanomaterials*, 10.3390/nano12152518
- [19] J. Lin, S. T. Pantelides, W. Zhou, *ACS Nano* **2015**, 9, 5189.
- [20] F. Arnold, R.-M. Stan, S. K. Mahatha, H. E. Lund, D. Curcio, M. Dendzik, H. Bana, E. Travaglia, L. Bignardi, P. Lacovig, D. Lizzit, Z. Li, M. Bianchi, J. A. Miwa, M. Bremholm, S. Lizzit, P. Hofmann, C. E. Sanders, *2D Materials* **2018**, 5, 045009.
- [21] a) J. Feng, D. Biswas, A. Rajan, M. D. Watson, F. Mazzola, O. J. Clark, K. Underwood, I. Marković, M. McLaren, A. Hunter, D. M. Burn, L. B. Duffy, S. Barua, G. Balakrishnan, F. Bertran, P. Le

- Fèvre, T. K. Kim, G. van der Laan, T. Hesjedal, P. Wahl, P. D. C. King, *Nano Letters* **2018**, 18, 4493; b)Y. Wang, J. Ren, J. Li, Y. Wang, H. Peng, P. Yu, W. Duan, S. Zhou, *Physical Review B* **2019**, 100, 241404.
- [22] Y.-C. Lin, D. O. Dumcenco, Y.-S. Huang, K. Suenaga, *Nature Nanotechnology* **2014**, 9, 391.
- [23] a)D. Li, X. Wang, C.-m. Kan, D. He, Z. Li, Q. Hao, H. Zhao, C. Wu, C. Jin, X. Cui, *ACS Applied Materials & Interfaces* **2020**, 12, 25143; b)Y. Wang, Z. Sofer, J. Luxa, M. Pumera, *Advanced Materials Interfaces* **2016**, 3, 1600433; c)G. V. Pushkarev, V. G. Mazurenko, V. V. Mazurenko, D. W. Boukhvalov, *Physical Chemistry Chemical Physics* **2019**, 21, 22647.
- [24] A. Zangwill, *Physics at Surfaces*, Cambridge University Press, Cambridge **1988**.
- [25] J. Cai, W. Jolie, C. C. Silva, M. Petrović, C. Schlueter, T. Michely, M. Kralj, T.-L. Lee, C. Busse, *Physical Review B* **2018**, 98, 195443.

Supporting information

Phase Transition of the single-layer vanadium diselenide on Au(111) with distinguished electronic structures

Jinbang Hu, Xiansi Wang, Chaoqin Huang, Fei Song, and Justin W Wells

Jinbang Hu

Department of Physics, Norwegian University of Science and Technology, NO-7491

Trondheim, Norway

E-mail: jinbang.hu@ntnu.no

Xiansi Wang

Hunan University, Changsha, 410082, China

Fei Song, Chaoqin Huang

Shanghai Advanced Research Institute, Chinese Academy of Sciences, Shanghai 201000,
China;

Justin W. Wells

Department of Physics, Norwegian University of Science and Technology, NO-7491

Trondheim, Norway

Semiconductor Physics, Department of Physics, University of Oslo (UiO), NO-0371 Oslo,
Norway

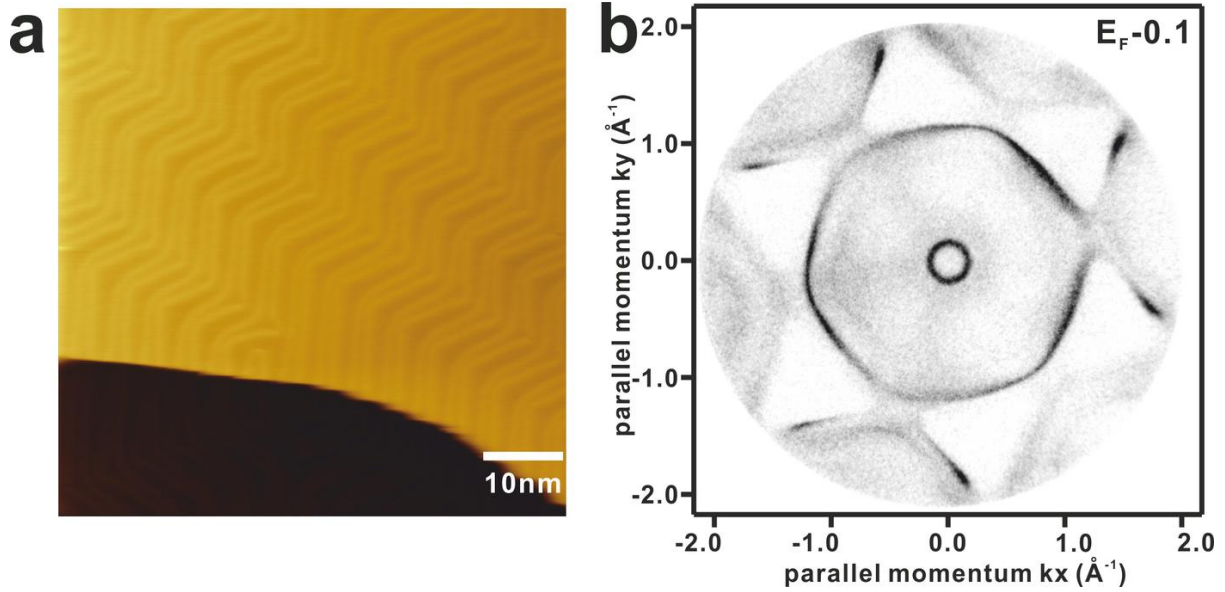


Figure. S1 (a) STM image of clean Au(111) surface. (b) ARPES data of constant energy contours throughout the surface Brillouin zone at 0.1 eV below the Fermi level.

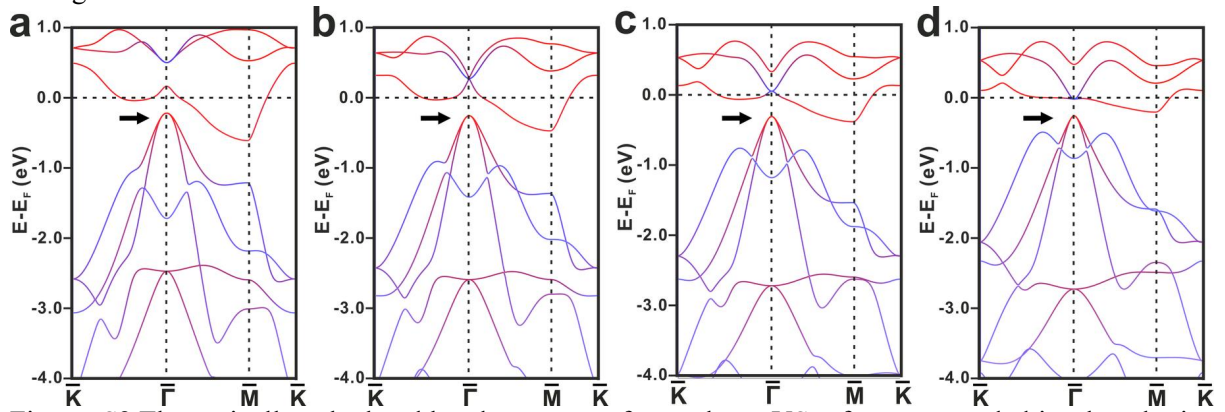


Figure. S2 Theoretically calculated band structure of monolayer VSe₂ for an expanded in-plane lattice parameters (a) 3.35 Å, (b) 3.55 Å, (c) 3.65 Å, (d) 3.75 Å, the relative energy position of the parabolically dispersing band around the Γ point is marked by the black arrow.

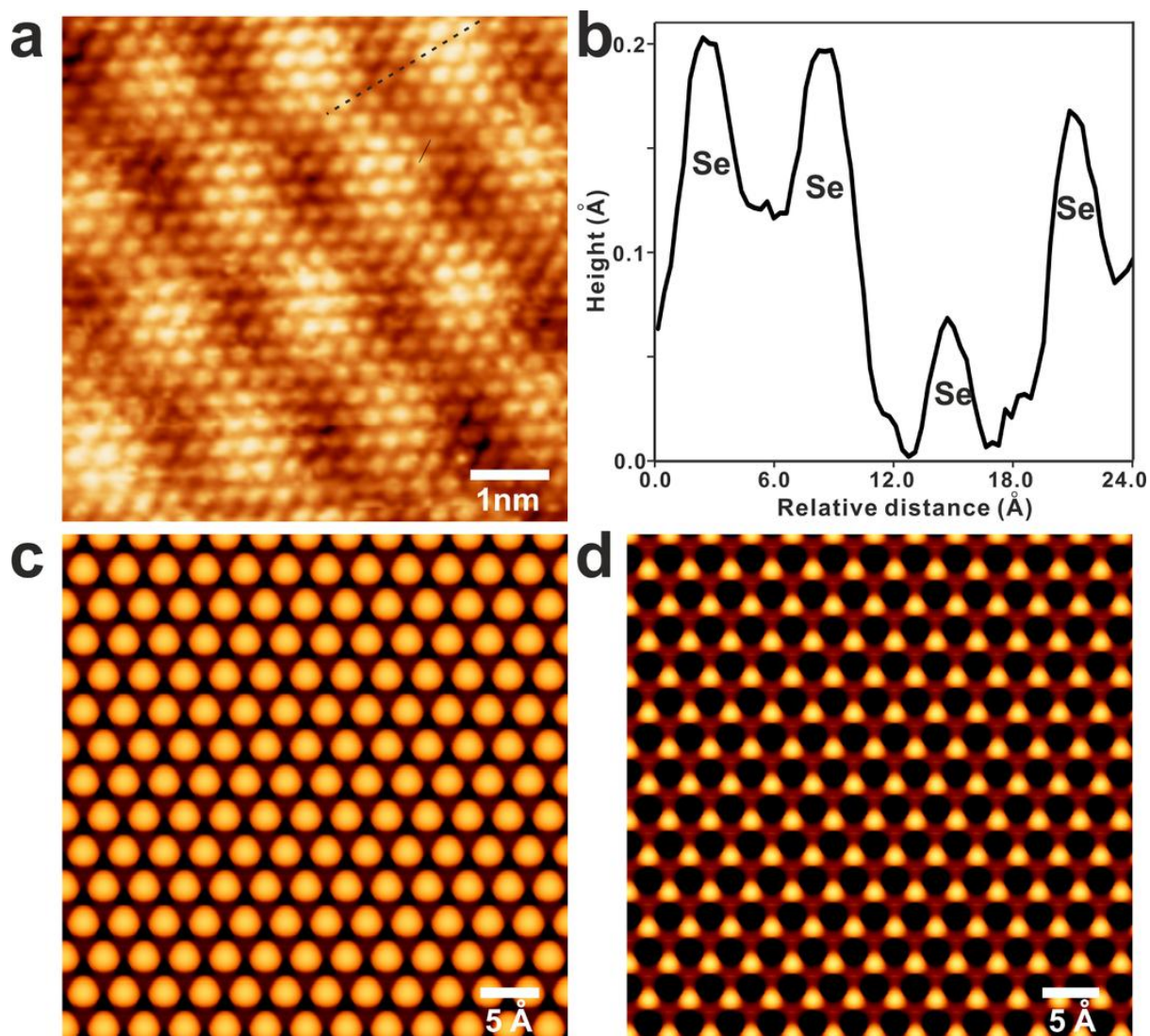


Figure. S3 (a) Atomic-resolution STM image of SL VSe₂ showing the hexagonal lattice of Se atoms in the topmost sublayer of the VSe₂ sandwich-type structure. (b) The intensity profile along the black dashed line marked in (a). (c) simulation of free standing 1T VSe₂ and (d) 2H VSe₂. Scanning parameters: $U = -1.2$ V and $I = 0.12$ nA.